



ELSEVIER

Atmospheric Research 63 (2002) 221–245

ATMOSPHERIC
RESEARCH

www.elsevier.com/locate/atmos

Aerosol climatology for the planetary boundary layer derived from regular lidar measurements

V. Matthias*, J. Bösenberg

Max-Planck-Institut für Meteorologie, Bundesstraße 55, D-20146 Hamburg, Germany

Received 12 February 2002; accepted 22 April 2002

Abstract

Regular aerosol extinction and backscatter measurements using a UV Raman Lidar have been performed for almost 3 years in Hamburg in the frame of the German Lidar Network. A set of 92 aerosol extinction and 164 aerosol backscatter profiles has been used for statistical investigations. Mean values and variances of the aerosol extinction and backscatter in the boundary layer have been calculated. Large fluctuations during the whole year have been found. The measured aerosol extinction over Hamburg shows a seasonal cycle with highest values in early fall and a second less prominent peak in spring. An analysis of the data using back trajectories showed a dependence of the aerosol extinction on the origin of the air mass. The residence time of the air mass over industrialized areas was found to be an important parameter for the measured aerosol extinction at Hamburg. However, only a small part of the total variability could be explained by the air mass origin. For 75 cases of aerosol extinction measurements under cloud-free conditions, the aerosol backscatter profile and therefore, the lidar ratio as a function of altitude could be determined. Winter measurements of the lidar ratio are often close to model results for maritime aerosol, the summer measurements are close to the model results for urban or continental aerosols. The high quality of the data has been proven by intercomparisons with other lidar systems and with star photometer measurements of the aerosol optical depth during the Lindenberg Aerosol Characterization Experiment (LACE'98) field campaign. © 2002 Elsevier Science B.V. All rights reserved.

Keywords: Lidar; Aerosol; Boundary layer; Climatology

1. Introduction

Atmospheric aerosols have large influence on the Earth's radiation budget. The IPCC (2001) estimated the possible impact of aerosols, direct and indirect effects, on the

* Corresponding author. Tel.: +49-40-41173-419; fax: +49-40-41173-359.

E-mail address: matthias@dkrz.de (V. Matthias).

radiative forcing (top of the atmosphere) in a global average in an order of magnitude which would almost compensate the CO₂ effect. However, high uncertainties, especially for the indirect effect, are connected with the aerosol influence on climate and even the smaller direct effect of aerosols is still not well understood.

Aerosols have relatively short lifetimes, they can be very complex in shape and chemical composition and they change their optical properties with relative humidity. Because the global aerosol distribution is very inhomogeneous, both horizontally and vertically, aerosols can have quite large effects in some regions of the Earth, whereas their influence is negligible in other regions. However, data on the spatial and temporal distribution are rather sparse. Satellite data cover most parts of the Earth (Herman et al., 1997) but are still of high uncertainty over land, where the main aerosol sources are (Kaufman et al., 1997). Additionally, it suffers from the poor vertical resolution (Kaufman et al., 1997) and the influence of clouds, which can prevent the observation of aerosol plumes completely. Sun photometers for the measurement of the total optical depth are now widely spread over the whole globe (Holben et al., 1998), but these measurements cannot deliver vertical resolution either and can only be performed when it is totally cloud-free. Therefore, winter data in mid-latitudes are not very frequent and there is definitely a “good weather” bias of those measurements. In situ measurements at ground level give only locally representative information on the aerosol distribution that cannot be used for the vertical dimension. Aircraft-based aerosol measurements could solve this problem but are very expensive and therefore, are only performed for short time intervals during field campaigns. So far, this was also true for lidar measurements which were mainly restricted to field campaigns (e.g., ACE-1, ACE-2, TARFOX, LACE'98) (Bates et al., 1998; Russell et al., 1999; Ansmann, in press), but in this paper, it is shown that lidars can also be operated for several years on a regular schedule.

Vertically resolved aerosol data are needed to complement satellite-based observations and ground-based sun photometer measurements (Kaufman et al., 1997). The operation of lidar systems on a routine basis is very valuable for a long-term observation of the aerosol vertical distribution. The aerosol vertical structure is at least a by-product of almost every lidar measurement, since already simple elastic backscatter signals at almost any lidar wavelength give a qualitative impression about the vertical aerosol distribution. However, these measurements are not quantitative, since the results depend on two guessed values: the lidar ratio and the calibration constant. This problem can be solved using the Raman lidar technique (Ansmann et al., 1992b) or scanning systems with the multiangle approach (Gutkowitz-Krusin, 1993). High spectral resolution lidar (HSRL) (Shipley et al., 1983; Grund and Eloranta, 1991) delivers aerosol extinction profiles even with high temporal resolution, but they require substantial technical effort. Therefore, those systems are very expensive and not easy to handle.

To get better data on the vertical and horizontal aerosol distributions in Germany, regular aerosol lidar measurements have been performed three times a week by a small lidar network of five stations in Germany (Bösenberg et al., 1998). At least one measurement per week included extinction determination by either the Raman method (three systems) or the multiangle approach (two systems). In the meantime, this network has been extended to a continental scale, 20 stations in Europe are operated within the EU-project EARLINET since May 2000 (Bösenberg et al., 2001).

For the harmonization of the data set and for quality control, intercomparison experiments have been performed between the lidar systems and with passive remote sensors. The measurements were done during the Lindenberg Aerosol Characterization Experiment (LACE'98) and included two other lidar systems as well as sun and star photometers. Several in situ instruments at ground level and on aircraft were also present.

For the routine observations at the Max-Planck-Institut für Meteorologie Hamburg, the Raman method has been used with an XeF excimer laser emitting at 351 nm. These aerosol extinction and backscatter profiles have been evaluated using statistical considerations. Frequency distributions have been derived, and mean, standard deviation and skewness of the distributions for aerosol extinction, aerosol backscatter, the lidar ratio and the optical depth have been calculated for the boundary layer on the basis of 92 extinction and 164 backscatter measurements between 1 December 1997 and 31 October 2000. The lidar ratio values have been compared to model results using Mie calculations for typical aerosols. An analysis of the origin of the air masses has been made using back trajectories.

2. Methods

2.1. Aerosol backscatter

Aerosol lidar measurements at one wavelength can deliver aerosol backscatter profiles using inversion techniques proposed, e.g. by Fernald et al. (1972), Fernald (1984) and Klett (1981). However, these techniques generally are not quantitative because they have certain errors (Sasano et al., 1985; Kovalev and Moosmüller, 1994; Matsumoto and Takeuchi, 1994). This is mainly due to the fact that the lidar equation contains two unknown aerosol parameters, the aerosol extinction and backscatter. All molecular parameters can be calculated with sufficient accuracy (Bodhaine et al., 1999) from ground values of pressure and temperature, but for solving the equation for the aerosol backscatter, a relationship between the unknown quantities (aerosol extinction and backscatter), the so-called lidar ratio, is assumed. It depends on the aerosol microphysics and can vary between less than 10 sr (ice crystals) and more than 100 sr (heavily polluted air) (Ackermann, 1998), it depends on humidity and aerosol mixture and therefore, on height. This value has to be guessed and can introduce large errors especially in cases with high aerosol optical depth. It is the main error source of pure elastic backscatter measurements in the UV and green.

The necessary calibration constant can be calculated at least at shorter wavelengths ($\lambda \lesssim 750$ nm) in regions with low aerosol backscatter, which is in many cases, the fact in higher altitudes of the troposphere, without introducing too large errors on the aerosol backscatter profile.

However, at 351 nm, one can get reasonable aerosol vertical profiles at daytime, although the accuracy of the aerosol backscatter in many cases is not better than 50%. At the MPI für Meteorologie, the Fernald algorithm is used, Rayleigh backscatter and extinction are calculated according to Elterman (1968) using ground values of temperature and pressure

and standard atmospheric conditions. If available, radiosonde data can also be used. The lidar ratio can be chosen height-dependent but usually a value of 50 sr, constant in height, is taken. This is a quite typical value in northern Germany. This value remains unchanged unless additional information is available or no reasonable profile can be calculated under that assumption.

2.2. Aerosol extinction

These problems with the aerosol backscatter determination can be solved by the additional measurement of the atmospheric Raman scattering on nitrogen or oxygen (Ansmann et al., 1992a). This allows the independent determination of the aerosol extinction:

$$\alpha_{\text{aer}}(\lambda_0) = \frac{1}{\left(1 + \left(\frac{\lambda_0}{\lambda_R}\right)^k\right)} \frac{d}{dz} \ln \left(\frac{N(z)}{P_R(z)z^2} \right) - \alpha_{\text{mol}}(\lambda_0, z) - \alpha_{\text{mol}}(\lambda_R, z), \quad (1)$$

where $\alpha_{\text{aer}}(\lambda_0, \lambda_R, z)$ and $\alpha_{\text{mol}}(\lambda_0, \lambda_R, z)$ are the height-dependent aerosol and molecular extinction at the emitted wavelength λ_0 and the Raman wavelength λ_R . $P_R(z)z^2$ is the range-corrected Raman signal and $N(z)$ is the density of the Raman scatterer, in this case, of atmospheric nitrogen. $N(z)$ is usually well known from ground values of temperature and pressure or even better, from nearby launched radiosondes. For the wavelength dependence of the aerosol extinction, a power law $\alpha_{\text{aer}}(\lambda) \propto \lambda^{-k}$ is assumed where the Ångström coefficient k is the only parameter which has to be guessed for the solution of Eq. (1). Its influence on the result remains small (Ansmann et al., 1992a; Whiteman, 1999), usually $k=1$ is chosen.

However, this technique is mostly limited to nighttime, since during daytime, the solar background light is much higher than the backscattered Raman signal. Therefore, the regular aerosol extinction measurements with the MPI lidar system have been performed right after sunset.

2.3. Lidar ratio

With an extinction profile from the Raman method, the aerosol backscatter profile can be determined without assumptions on the lidar ratio. In cases where at least broken clouds allow a calibration of the lidar signal in a region of the atmosphere with very low aerosol backscatter, the aerosol backscatter profile is calculated using the extinction information and the assumption about the total backscatter in the calibration height z_0 :

$$\beta_{\text{aer}}(\lambda_0, z) = -\beta_{\text{mol}}(\lambda_0, z) + (\beta_{\text{aer}}(\lambda_0, z_0) + \beta_{\text{mol}}(\lambda_0, z_0)) \times \frac{P(\lambda_0, z)z^2}{P(\lambda_0, z_0)z_0^2} \exp \left(-2 \int_z^{z_0} (\alpha_{\text{aer}}(\lambda_0, \zeta) + \alpha_{\text{mol}}(\lambda_0, \zeta)) d\zeta \right). \quad (2)$$

Here, $\beta_{\text{aer}}(\lambda_0, z)$ is the height-dependent aerosol backscatter from the wavelength λ_0 .

From these two profiles, an altitude-dependent lidar ratio

$$S = \alpha_{\text{aer}}(\lambda_0, z) / \beta_{\text{aer}}(\lambda_0, z) \quad (3)$$

can be calculated for all cases where a calibration of the elastic backscattered signal is possible. Only if the sky is completely covered with low clouds that do not allow getting backscattered signals from regions of the atmosphere with low aerosol content, the lidar ratio cannot be determined.

Table 1

The MPI aerosol lidar system: detailed technical information on the configuration used for routine measurements within the German Lidar Network

Emitter		
Laser type	Lambda Physik EMG 201, XeF excimer	
Emitted wavelength	351 nm	
Typical energy	50 mJ	
Repetition rate (typical)	10–20 Hz	
Beam expansion	threefold	
Beam divergence	<0.2 mrad	
Receiving optics		
	Telescope 1	Telescope 2
Diameter	400 mm	150 mm
Focal length	1400 mm	450 mm
Field stop	1.25-mm quartz fibre	
Scanning capability	no	
Zenith angle	0°	
Beam/telescope configuration	biaxial	
Wavelength separation	beam splitter	
Detectors		
Elastic channels		
Wavelength	351 nm	
Detector	PMT, EMI 9883 QB	
Preamplifier	FEMTO HCA-S	
Filter bandwidth	10 nm	
Raman channels		
Wavelength	382 nm	
Detector	PMT, EMI 9893 QB 350	
Discriminator	Phillips Scientific 6904	
Data acquisition mode	700 MHz photon counting, Optech FDC700M	
Filter bandwidth	1.5 nm	
Data acquisition		
	Elastic	Raman
Acquisition system	12-bit analog	700 MHz photon counting
Manufacturer	PENTEK	Optech
Range resolution (raw)	15 m	30 m
Time resolution analysis (raw)	10 s	30 s
Continuous acquisition	yes	yes

2.4. Regular measurements

Having these considerations in mind, it was decided in the German Lidar Network to perform three measurements per week on fixed days. If rain, fog or too low clouds prevented lidar measurements within a given time window, no measurement has been made on that day and the reason for this was recorded. Originally, two aerosol backscatter measurements on Monday and Thursday afternoons, when the boundary layer is fully developed, and one extinction measurement on Monday evenings were planned. These measurements started on 1 December 1997. During the project, it became clear that the evening measurements of the aerosol extinction are much more valuable than the backscatter measurements in the afternoon, so from 1 January 2000, the Thursday afternoon measurement was shifted to Thursday evening. The measurements were taken between 1 h before and 3 h after sunset. At that time, the planetary boundary layer (PBL) usually is still fully developed and the measurements represent the afternoon PBL quite well.

3. MPI aerosol lidar

The aerosol lidar system of the MPI für Meteorologie is based on an XeF excimer laser emitting at 351 nm. The laser beam is expanded three times and then vertically emitted into the atmosphere.

Equipped with two receiving telescopes, the height range covered with aerosol backscatter measurements is from ca. 300 to 10,000 m. Measurements of the Raman backscatter on atmospheric nitrogen at 382 nm are used to determine the aerosol extinction profile in altitudes between ca. 500 and 5000 m.

In the Raman channel, a PMT with small cathode area is used to reduce dark counts. Elastic backscatter signals are detected in analog mode with 12-bit analog–digital converters (ADC) with a typical resolution of 15 m in the vertical and 10 s in time. The photon-counting system used for the Raman channel has a height resolution of 30 m and a typical time resolution of 30 s. The measured dead time of the receiving detector and the following electronics is in the order of 8–11 ns, leading to maximum useful count rates of ca. 20 MHz.

The whole system is built in a standard 20-ft container and can be transported. It has been used for routine measurements at Hamburg within the German Lidar Network and for the LACE'98 field campaign at Lindenberg (Ansmann, *in press*). Detailed information can be found in Table 1.

4. Data quality assurance

For quality assurance of the data, intercomparisons between the lidar systems participating in the German Lidar Network have been made. In summer of 1998, the MPI lidar was located in Lindenberg/Brandenburg to participate in the Lindenberg Aerosol Characterization Experiment (LACE'98) (see, e.g. Wandinger *et al.*, *in press*), together with two other aerosol lidar systems from the Institut für Troposphärenforschung (IfT) Leipzig (Althausen *et al.*, 2000) and the Meteorologisches Institut der Universität Munich

(MIM) (Wiegner et al., 1995) which are also part of the German Lidar Network. Several measurements on different days and times have been compared to ensure the high quality of the derived aerosol profiles. Here, two examples are presented.

In Fig. 1, the intercomparison of aerosol backscatter profiles of the MPI lidar with the MIM and the IfT lidars at UV wavelengths can be seen. For these profiles, common lidar ratios have been used, but each group has processed their own data. The agreement is remarkably good in altitudes above 1400 m. The deviations to the IfT lidar below that height result most likely from overlap effects in the IfT lidar. Fig. 2 shows an intercomparison of aerosol extinction profiles derived with the Raman method between the MPI lidar system and the multi-wavelength lidar of the IfT Leipzig. There is excellent agreement over the whole altitude range. The mean deviation up to 2300 m is 5% with a standard deviation of 12%. The measurements performed by the MIM with the dual angle method are average values for the layers marked by the vertical bars. The ground value has been determined by using the slope method (see, e.g. Bösenberg et al., 1997). Those values have been taken in a short time interval of a few minutes around 21:50 UT. Having this in mind, the discrepancies between MPI and MIM, which are in the order of 15–20%, are quite low.

Additionally, the integrated extinction has been compared to star photometer measurements performed in Lindenberg by the German Weather Service. Three periods of 80 min between 11 August 1998, 22:20 UT and 12 August 1998, 2:20 UT have been taken for the intercomparisons. The extinction profiles showed a decreasing aerosol extinction between 1000 and 2000 m above sea level (asl). The lowest measurement point in 600 m has been

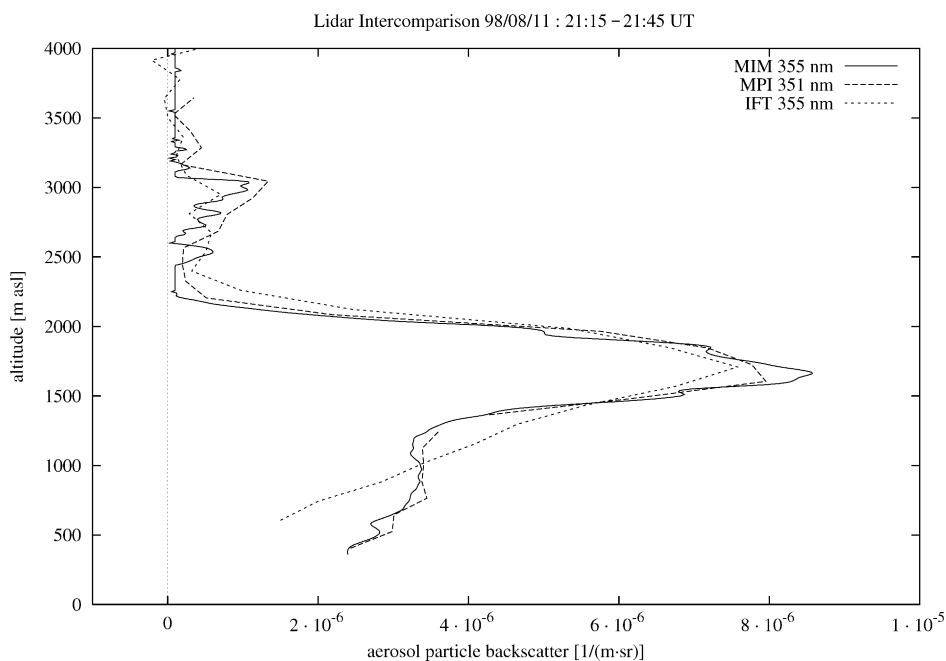


Fig. 1. Intercomparison of aerosol backscatter in the UV at 355 nm (IfT and MIM at 355 nm and MPI at 351 nm) during LACE'98.

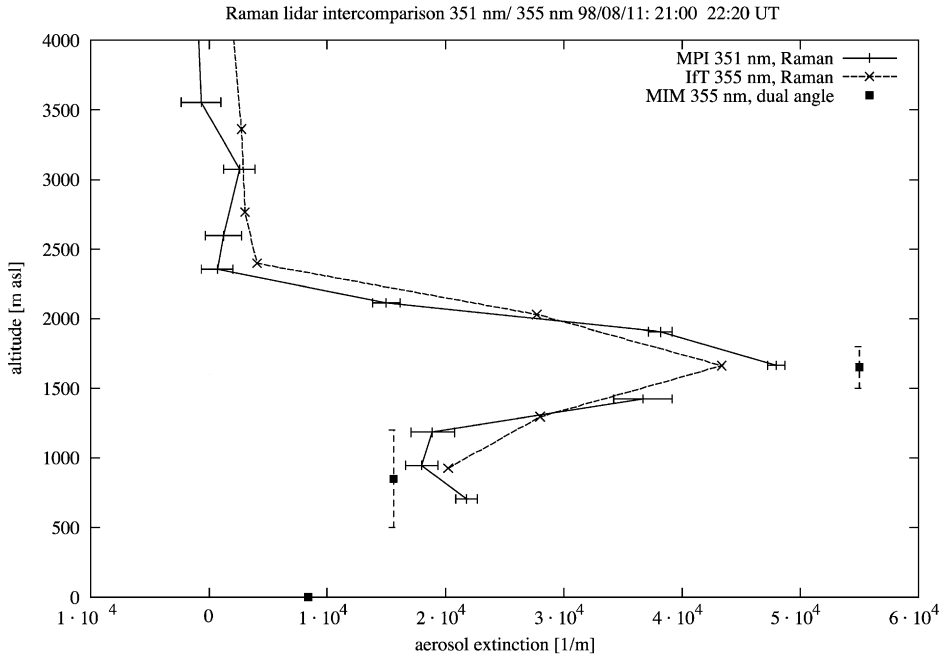


Fig. 2. Intercomparison of aerosol extinction profiles at 355 nm (IfT) and 351 nm (MPI) during LACE'98.

linearly extrapolated to ground to derive the integrated extinction over the whole height range. The optical depth in altitudes above 7000 m was assumed to be negligible since the stratosphere was very clean at that time and no cirrus clouds were detected with the lidar.

The star photometer measurements were taken between ca. 400 and 1000 nm and then extrapolated to 350 nm. Fig. 3 shows the decreasing optical depth, from 0.42 to 0.25 at 391 nm, during 4 h. From the lidar data, one knows that this was only due to the decreasing extinction in the layer between 1000 and 2000 m asl. The agreement of the lidar-derived optical thickness with the star photometer is very good, within the error bars of ca. 10%. These error bars include the statistical error of the lidar measurements and an error estimated to 25% in the layer below 600 m caused by the extrapolation of the lowest extinction value to the ground.

For these results, the overall accuracy of the extinction measurements can be specified to ca. 10–15%, a value which is mainly determined by the statistical error.

5. Climatology

5.1. Measurement statistics

Regular aerosol lidar measurements have been performed in Hamburg three times a week starting on 1 December 1997. In Table 2, the measurement statistics can be seen. For

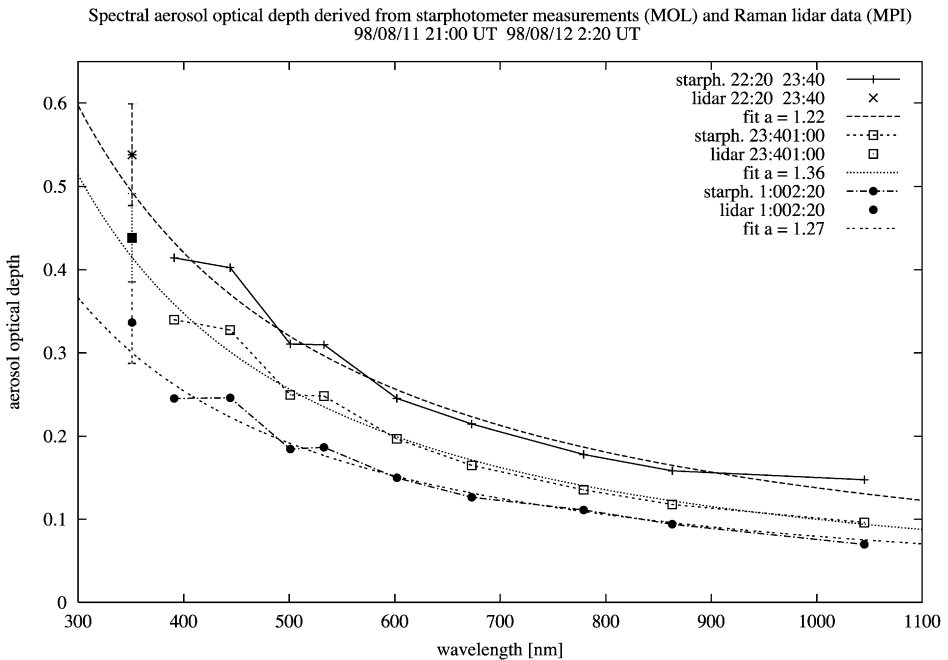


Fig. 3. Intercomparison of aerosol optical depth at 351 nm (MPI) and star photometer measurements from the Meteorologisches Observatorium Lindenberg (MOL) during LACE'98.

this statistics, only measurements from days of routine measurements with lowest clouds in about 800 m were taken. These measurements were divided into two classes. Class 1 consists of all measurements containing no permanent clouds below 2000 m. Sometimes, even small gaps between clouds are sufficient to determine a backscatter profile up to high altitudes. So, all cases without clouds and those with at least small cloud gaps are named “cloudfree.” In class 2, cloud coverage was present during the whole measurement period with clouds at altitudes below 2000 m. During the almost 3 years from 1 December 1997 to 31 October 2000, 276 routine measurements could be made, which is ca. 63% of all possible measurements. The intercomparison time, when the lidar was located in Lindenberg, has not been included in the number of possible measurements between April and September 1998. On 37% of the days, no measurements were possible. The reason for this was that mainly bad weather (26%), technical problems (5%) and public holidays (6%) did not play a major role for the prevention of measurements.

From all performed measurements, complete cloud coverage below 2000 m was present in only 16% of the cases. These measurements have to be handled carefully, since a correct calibration of the backscatter profile is very difficult, if a region of the atmosphere with very low aerosol content cannot be reached. On the other hand, this is not true for the aerosol extinction measurements with the Raman method, which are not dependent on calibration and can also be taken during complete cloud coverage.

Table 2

Measurement statistics for the MPI Hamburg on the basis of calculated backscatter profiles on routine measurement days (Monday afternoons and evenings, Thursday afternoons)

Measurements (1 December 1997–31 October 2000)						
Months	Possible measurements	Performed measurements	Performed/possible measurements (%)	Class 1	Class 2	Class 1/performed measurements (%)
December 1997– March 1998	53	31	58.5	20	11	64.5
April 1998– September 1998	55	43	78.2	35	8	81.4
October 1998– March 1999	79	48	60.8	35	13	72.9
April 1999– September 1999	79	58	73.4	54	4	93.1
October 1999– March 2000	78	42	53.8	38	4	90.5
April 2000– September 2000	78	48	61.5	45	3	93.8
October 2000	14	6	42.9	6	0	100.0
All	436	276	63.3	233	43	84.4

Class 1 summarizes all cases where measurement without low clouds were possible, class 2 measurements were affected by complete cloud coverage below 2000 m.

These numbers stress the fact that lidar is a suitable instrument for routine observations even in northern Germany, which is commonly believed to be a place with mainly bad weather. Even in winter, 57% of all possible measurements could be performed, although complete cloud coverage below 2000 m occurred in 23% of the cases, clearly more frequently than in summer (11%).

5.2. Aerosol extinction and backscatter

In almost all cases, the aerosol backscatter or extinction could be measured within the planetary boundary layer. Within this layer, highest aerosol concentrations can be found because this layer has per definition contact to the ground and almost all aerosol sources are at ground level. In only two cases, the top of the boundary layer was below the lowest measurement height, which is ca. 500 m for extinction profiles and 300 m for backscatter profiles. These cases have not been used for the statistics. A main bias of the winter measurements due to the limited range can be excluded due to the small number of not-considered measurements.

Separate statistics have been made for aerosol backscatter and aerosol extinction measurements. During the first 2 years, extinction profiles have been taken once a week on Monday evenings. Starting in January 2000, measurements have been made also on Thursday evenings to get a larger data set. Ninety-two profiles are forming the basis for the extinction statistics. Since these measurements do not need to be calibrated in an aerosol-free region, the statistics include measurements from both defined classes.

For the 92 extinction profiles, the average aerosol extinction in the boundary layer has been calculated by integrating the aerosol extinction up to the top of the boundary layer (which gives the aerosol optical depth) and then dividing the optical depth by the boundary layer height. The lowest extinction value was assumed to be representative down to the ground. This is a very reasonable assumption, since the boundary layer is still fully developed at sunset. Only turbulence has decreased and no further mixing can be observed.

Out of the backscatter measurements performed on routine observation days, generally, the afternoon measurement has been taken for the statistics. If, on some days, only evening measurements were possible due to bad weather in the afternoon, these measurements have additionally been taken. On the other hand, all measurements under low cloud conditions have been sorted out due to the high errors that are connected with the calibration under those conditions. In summary, 164 measurement days could be used for the statistics, which is 54% of all possible days within the almost 3 years.

Average aerosol backscatter values have been determined similar to the extinction taking the integrated aerosol backscatter up to the top of the PBL and then dividing by the PBL height. Looking at these measurements, one has to have in mind that the calculated aerosol backscatter profile depends on the chosen lidar ratio, which is not known without additional extinction measurement. Most of the afternoon backscatter profiles have therefore been calculated with a lidar ratio of 50 sr, a quite typical value in northern Germany (see Section 5.3).

Fig. 4 gives examples of aerosol extinction profiles derived with the Raman method. The profiles are scaled in height to the top of the boundary layer z_i , which can be clearly seen in the lidar signal and in the aerosol profiles. In most cases, the aerosol extinction and backscatter in the boundary layer is much higher than above it, so a steep gradient in the logarithm of the range-corrected backscattered signal can be seen. If the aerosol in the PBL in the afternoon is convectively mixed, the top of this layer shows characteristic fluctuations caused by individual turbulence elements. In these cases, the PBL can be easily identified. However, in 14 cases within the 3 years of measurements, a second aerosol layer above the boundary layer could be seen, e.g. on 7 September 1998 in Fig. 4. Those layers have not been included here in the presented statistics for the planetary boundary layer.

The annual cycle of the mean aerosol extinction in the boundary layer in Hamburg on the basis of 92 measurements from 1 December 1997 to 31 October 2000 can be seen in Fig. 5. A 6-week gliding average is also plotted, showing only small variations in the gliding average between October and June with a not very pronounced “spring maximum” in April. In the late summer, between July and September, the average aerosol extinction in the PBL is remarkably higher than during the rest of the year, with a maximum in September with values roughly twice the average of the other months. However, these high values refer mostly to very high values in September 1999, which was exceptionally hot and dry in Hamburg. Because up to now, only 3 years of measurements could be taken for this figure, this feature is still of high uncertainty. Further measurements will be taken at least up to the end of 2002 within the project “A European aerosol research lidar network to establish an aerosol climatology—EAR-LINET” (Bösenberg et al., 2001). That will give an even better data basis.

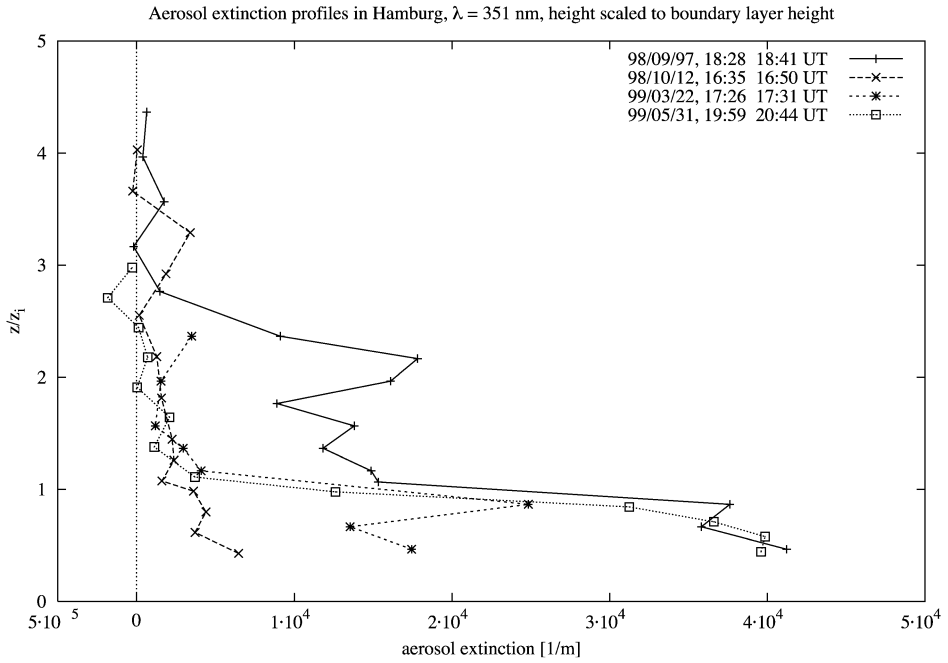


Fig. 4. Examples of aerosol extinction profiles measured in Hamburg in 1998 and 1999. The height z is scaled to the boundary layer height z_1 .

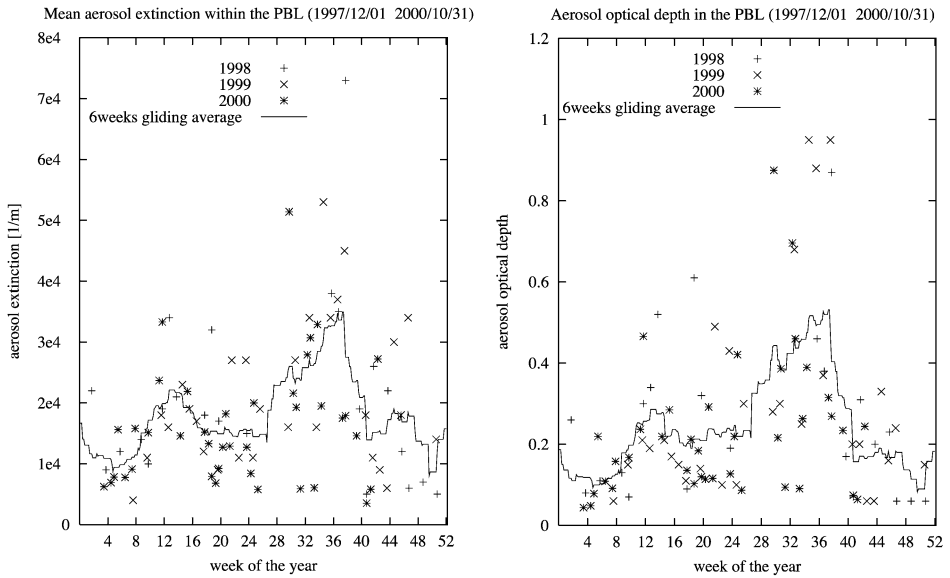


Fig. 5. Annual cycle of the average aerosol extinction and the optical depth in the boundary layer in Hamburg taking data from 1 December 1997 to 31 October 2000.

In Fig. 5, one additionally recognizes slightly lower values in winter than in summer and a wide spread of measured values during the whole year. Very low extinction values can appear in summer months as well as in winter months. On the other hand, very high values are mostly limited to April–September.

The annual cycle of the optical depth (Fig. 5, right side) is more pronounced than that of the average extinction. This is due to the inclusion of the boundary layer height which is generally much lower in winter than in summer. The other features remain the same.

Looking at the annual cycle of the aerosol backscatter (Fig. 6), the picture is very similar. The average aerosol backscatter in the boundary layer shows only small seasonal variations with a maximum in late summer and a less pronounced maximum in early spring. Again, remarkable is the wide spread of values with maximum values occurring in summer. The integrated aerosol backscatter, which is defined in analogy to the optical depth, shows a more pronounced annual cycle since PBL heights are much smaller in winter than in summer.

Fig. 7 displays the PBL height determined from the afternoon backscatter measurements. The gliding average shows a maximum of ca. 2000 m in midsummer and a minimum of ca. 900 m in midwinter. The sinus fit shows a small phase shift of 19 days against the yearly cycle of incoming solar radiation. The highest PBL can be expected around 10 July, the lowest around 9 January. The real PBL height can of course be very different from those statistical values. The standard deviation of the average value of 1510 m is 599 m (40%). Although the sinus fit can represent the annual cycle to be very good on the average, the standard deviation of the individual values is only reduced to 499 m (33%). This illustrates the high day-to-day variation of the PBL.

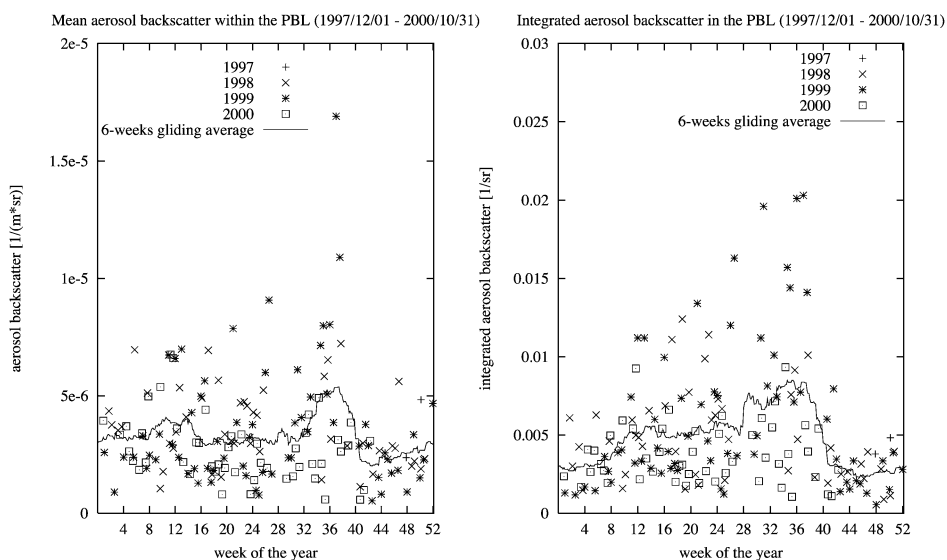


Fig. 6. Annual cycle of the average aerosol backscatter and the integrated aerosol backscatter in the boundary layer in Hamburg taking data from 1 December 1997 to 31 October 2000.

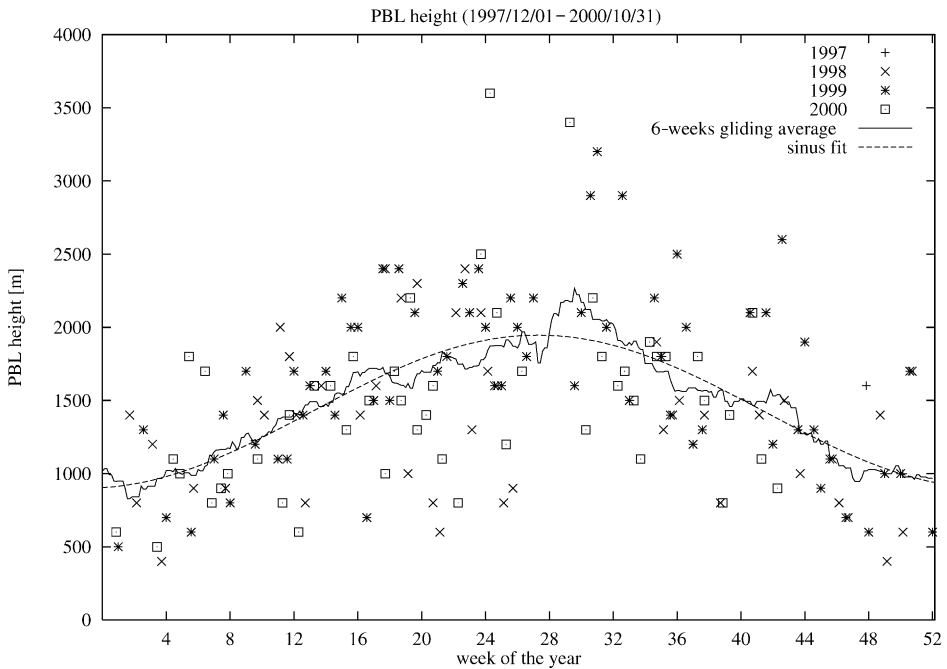


Fig. 7. Planetary boundary layer (PBL) heights derived from 164 aerosol backscatter measurements between 1 December 1997 and 31 October 2000. Also shown is a 6-week gliding average and a sinus fit which shows a phase shift of 19 days.

For the PBL height, the aerosol extinction and backscatter values, the statistical distributions have been derived. The characteristic quantities of the distributions are displayed in Table 3 (for extinction), Table 4 (for backscatter) and Table 5 (for PBL-height). For aerosol extinction and backscatter, one recognizes very similar averages in the years 1998 and 1999 and lower values in 2000. The PBL height shows highest values in 1999, and this is also recognized in the integrated backscatter and the aerosol optical depth. The interannual variation is less than $\pm 20\%$, only for the integrated backscatter, it is slightly higher. For the PBL height, it even stays in the order of $\pm 10\%$.

The standard deviation of the individual aerosol measurements is quite high, usually in the order of 50% or higher. This represents the fluctuations in aerosol extinction and backscatter, which can occur in quite short time intervals of a few hours. For the PBL height, it is in the order of 40%.

All distributions show positive skewness (γ -values), with high values being more frequent than low ones, as is typical for many meteorological quantities with only positive values. Again, the exception is the PBL height, which only in 2000, shows a remarkable positive skewness. This is at least partly due to the missing values in November and December 2000, which were most likely low.

The distribution of the PBL heights can be represented by a Gaussian distribution with a mean value and standard deviation given in Table 5. This is indicated by the low γ -value

Table 3

Characteristic quantities of the frequency distribution of the aerosol extinction (in 10^{-4} m^{-1}) and the optical depth in the boundary layer in Hamburg

Category	μ (10^{-4} m^{-1})	σ (10^{-4} m^{-1})	γ	Median (10^{-4} m^{-1})
<i>Aerosol extinction</i>				
1 December 1997–31 October 2000	1.87	1.21	1.59	1.65
1998	2.05	1.50	1.87	1.95
1999	2.09	1.18	0.91	1.85
2000 (January–October)	1.60	1.00	1.34	1.50
Summer	2.21	1.35	1.49	1.85
Winter	1.47	0.86	0.78	1.25
<i>Optical depth</i>				
1 December 1997–31 October 2000	0.28	0.23	1.57	0.205
1998	0.26	0.21	1.30	0.195
1999	0.30	0.25	1.58	0.205
2000 (January–October)	0.23	0.18	1.78	0.185
Summer	0.34	0.25	1.18	0.27
Winter	0.16	0.10	0.83	0.155

It has been distinguished between the years and between summer and winter. μ : average, σ : standard deviation, γ : skewness.

Table 4

Characteristic quantities of the frequency distribution of the aerosol backscatter (in $10^{-6} \text{ (m sr)}^{-1}$) and the integrated backscatter (in 10^{-3} sr^{-1}) in the boundary layer in Hamburg

Aerosol backscatter				
Category	μ [$10^{-6} \text{ (m sr)}^{-1}$]	σ [$10^{-6} \text{ (m sr)}^{-1}$]	γ	Median [$10^{-6} \text{ (m sr)}^{-1}$]
1 December 1997–31 October 2000	3.37	2.15	2.20	2.90
1998	3.64	1.63	0.47	3.20
1999	3.64	2.79	2.14	2.60
2000 (January–October)	2.79	1.39	0.85	2.70
Summer	3.62	2.47	2.19	3.10
Winter	3.04	1.56	0.81	2.80
Integrated backscatter				
Category	μ [$10^{-3} \text{ (m sr)}^{-1}$]	σ [$10^{-3} \text{ (m sr)}^{-1}$]	γ	Median [$10^{-3} \text{ (m sr)}^{-1}$]
1 December 1997–31 October 2000	5.00	3.79	1.80	3.90
1998	4.88	2.95	0.82	4.30
1999	6.04	4.99	1.31	3.90
2000 (January–October)	3.79	1.91	0.92	3.30
Summer	6.18	4.34	1.38	5.00
Winter	3.41	2.03	1.35	3.10

It has been distinguished between the years and between summer and winter. μ : average, σ : standard deviation, γ : skewness.

Table 5

Characteristic quantities of the frequency distribution of the planetary boundary layer height in Hamburg

PBL height				
Category	μ (m)	σ (m)	γ	Median (m)
1 December 1997–31 October 2000	1509	599	0.57	1520
1998	1345	529	0.19	1420
1999	1644	613	0.14	1620
2000 (January–October)	1483	609	1.24	1520
Summer	1751	570	0.58	1720
Winter	1184	471	0.54	1120

It has been distinguished between the years and between summer and winter. μ : average, σ : standard deviation, γ : skewness.

and the median being almost equal to the mean. Fig. 8 shows the good agreement of the measured cumulative frequency distribution with the calculated Gaussian distribution.

The situation is different for the distribution of the aerosol extinction and backscatter, the aerosol optical depth and the integrated backscatter. High skewness and a much lower median than mean show that the distributions of these values are not Gaussian. Good agreement with calculated distributions can be achieved when using lognormal distributions of the form

$$f(x) = \frac{1}{sx\sqrt{2\pi}} \exp\left(-\frac{(\ln x - m)^2}{2s^2}\right) \quad (4)$$

which means that $\ln x$ follows a Gaussian (or normal) distribution with mean m and standard deviation s . The median of the distribution is then given by e^m . The values for m and s , which represent the measured distributions, can best be seen in Table 6. The

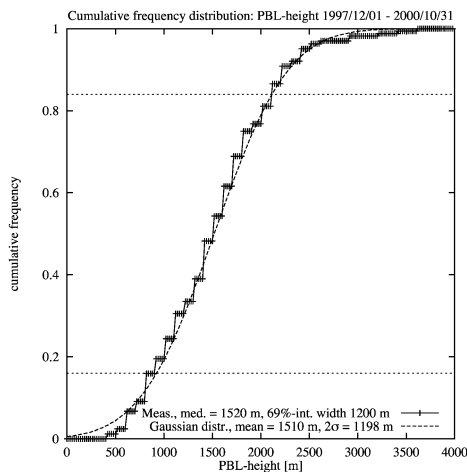


Fig. 8. Cumulative frequency distribution of the boundary layer height in Hamburg including data from 1 December 1997 to 31 October 2000. The mean is 1509 m with a 69% interval width of 1198 m. A Gaussian distribution using the μ - and σ -values from Table 5 are plotted.

Table 6

Characteristic quantities of the lognormal distributions that fit best to the measured values of aerosol extinction and backscatter, aerosol optical depth and integrated backscatter

Parameters of lognormal distributions			
Quantity	m	s	Median
Aerosol extinction	-8.77	0.630	$1.54 \times 10^{-4} \text{ m}^{-1}$
Optical depth	-1.64	0.753	0.194
Aerosol backscatter	-12.77	0.603	$2.83 \times 10^{-6} (\text{m sr})^{-1}$
Integrated backscatter	-5.54	0.698	$3.92 \times 10^{-3} \text{ sr}^{-1}$

cumulative frequency distributions of the lognormal distributions are plotted together with the measured values in Figs. 9 and 10. The deviations between measured and calculated distributions are small.

The goodness of all fitted distributions has been tested using both the χ^2 test and the Kolmogorov–Smirnov test on a 95% significance level. For this purpose, the data have been divided into nine classes in order to have the required number of five or more elements in each class. For the χ^2 test, the sum of the relative deviations of the class population from the values derived from the fit is calculated. The Kolmogorov–Smirnov test looks for the maximum deviation a of the cumulative frequency distribution from the fit values. The maximum allowed values for χ^2 and a depend on the number of data points and the chosen number of classes. They can be derived from tables (see, e.g. Johnson and Leone, 1964). The results together with the required χ^2 and a -values are displayed in Table 7. In all cases, the calculated values are much lower than the requirements for a good fit on the 95% significance level. Therefore, the selected functions represent the measured values

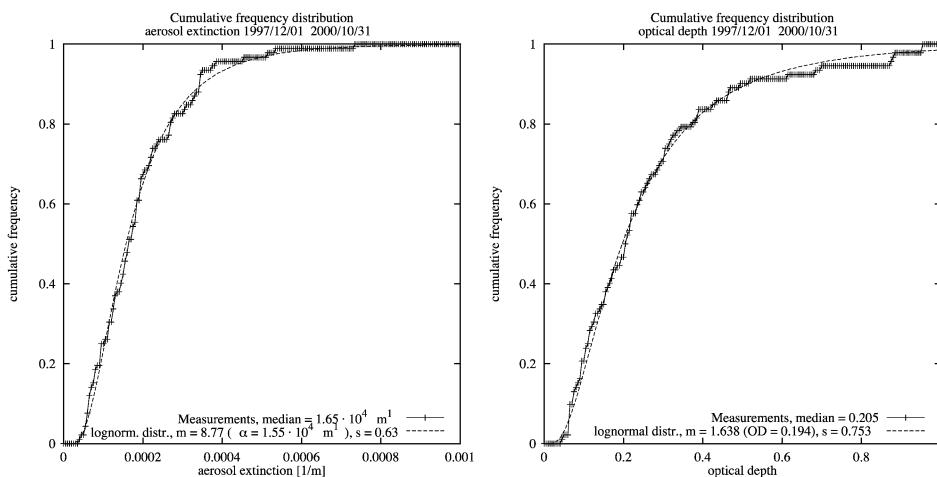


Fig. 9. Cumulative frequency distribution of the mean aerosol extinction (left side) and the optical depth (right side) in the boundary layer in Hamburg including data from 1 December 1997 to 31 October 2000. For extinction, the median is $1.65 \times 10^{-4} \text{ m}^{-1}$ with a 69% interval width of $2.4 \times 10^{-4} \text{ m}^{-1}$. The optical depth has a median of 0.205 with a 69% interval width of 0.34. In both pictures, lognormal distributions using the m - and s -values from Table 6 are also plotted.

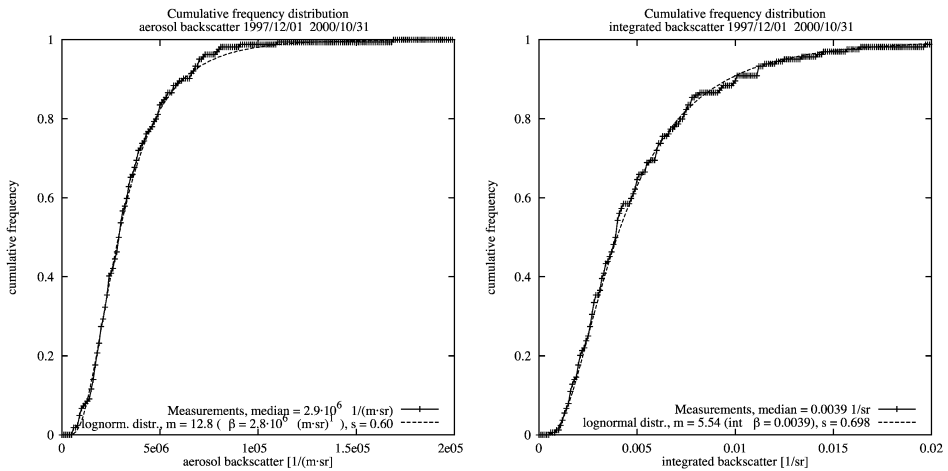


Fig. 10. Cumulative frequency distribution of the mean aerosol backscatter (left side) and the integrated backscatter (right side) in the boundary layer in Hamburg including data from 1 December 1997 to 31 October 2000. For backscatter, the median is $2.9 \times 10^{-6} \text{ (m sr)}^{-1}$ with a 69% interval width of $3.4 \times 10^{-6} \text{ (m sr)}^{-1}$. The integrated backscatter has a median of $4.0 \times 10^{-3} \text{ sr}^{-1}$ with a 69% interval width of $5.8 \times 10^{-3} \text{ sr}^{-1}$. In both pictures, lognormal distributions using the m - and s -values from the Table 6 are also plotted.

to be very good. Deviations of the data from the fit can be regarded as statistically not significant.

Part of the variability of the data (between 5% and 25% in σ/μ) can already be explained by distinguishing between two seasons only, October–March (winter) and April–September (summer). The lower values of the aerosol extinction and backscatter in winter can be seen in the mean and the median. Since very high aerosol extinction is measured mainly in summer, the skewness and the standard deviation of both semiannual distributions are reduced compared to the overall distribution. This is especially significant for the integrated values and in winter with more than 20% variability reduction. In summer, the variability reduction is much smaller, the standard deviation of the summer backscatter values is even a little higher than the overall standard deviation.

Table 7

Results of two common goodness-of-fit tests (χ^2 test and Kolmogorov–Smirnov test) on a 95% significance level

Goodness-of-fit test (95% significance level)

Parameter	Fitted distribution	Calculated χ^2	Allowed χ^2	Calculated a	Allowed a
Aerosol extinction	lognormal	3.16	14.07	0.041	0.144
Optical depth	lognormal	9.27	14.07	0.060	0.144
Aerosol backscatter	lognormal	5.15	14.07	0.036	0.106
Integrated backscatter	lognormal	1.15	14.07	0.034	0.106
PBL height	Gaussian	11.45	14.07	0.030	0.106

Deviations of the data from the fit are not significant on the given level if the calculated values stay below the given limits.

Table 8
Lidar ratio statistics for all values and distinguished into seasons

Lidar ratio						
Category	μ	σ	γ	σ/μ	Median	n
1998–2000	63	34	2.16	0.54	59	339
Summer	69	34	2.62	0.49	64	245
Winter	48	30	1.19	0.62	41	94

μ : mean, σ : standard deviation γ : skewness, σ/μ : relative standard deviation of the individual value, n : number of used independent values.

5.3. Lidar ratio

In 75 cases, an aerosol backscatter profile based on the extinction evaluation has been calculated. Only measurements where a reliable calibration of the backscatter profile could be made have been taken for the lidar ratio statistics (Table 8).

All independent lidar ratio values (339) in the boundary layer have been statistically evaluated, similar to the aerosol extinction. The histogram (Fig. 11) shows a higher probability for lower values in winter than in summer. The mean values are 63 sr for all values, 69 sr in summer and 48 sr in winter. Again, these values are high compared to the most probable values, in winter, the median is 41 sr, in summer, it is 64 sr. Sixty-nine percent of the values in summer are between 45 and 91 sr, and in winter between 21 and 81 sr.

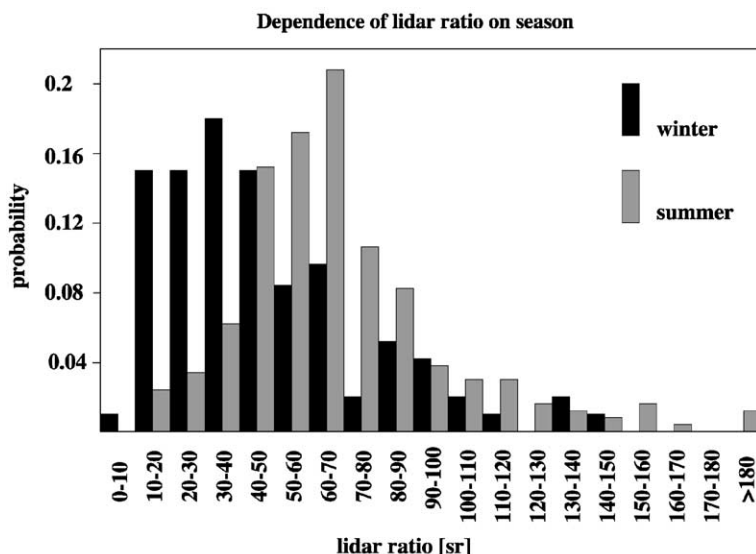


Fig. 11. Probability histogram of the lidar ratio in steps of 10 sr, distinguished between summer (245 values) and winter (94 values).

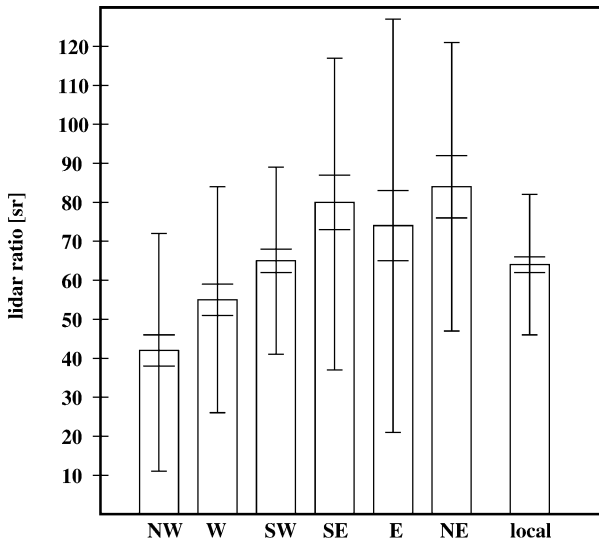


Fig. 12. Mean lidar ratio depending on the origin of the air mass. Inner error bars represent the standard deviation of the average, outer error bars of individual value.

The lidar ratio depends on the microphysical properties of the scattering aerosol particles (Fig. 12). Model results based on Mie calculations (Ackermann, 1998) show values between 20 and 30 sr for maritime aerosols and between 60 and 70 sr for urban aerosols. On the average, the model fits well with the measured values. This gives some indication that the lidar ratio could be used for the characterization of the aerosols. It should at least be possible to distinguish between sea salt-dominated aerosols with low lidar ratio and more urban soot containing aerosols with higher lidar ratio.

Very few of the measured values showed lidar ratios larger than 120 sr, they occurred mainly in summer. This might be due to an exceptionally high soot amount of the observed aerosol, resulting in high absorption values and therefore, high extinction to backscatter ratios. On the other hand, especially the lidar ratio is connected with relatively high error margins due to the statistical error of both the aerosol extinction and backscatter and a calibration error in the backscatter.

6. Air mass analysis

To explain the variability of the aerosol load at Hamburg, a separation into summer and winter has been made in the previous section. This separation is rather coarse and can only reduce the variability of the aerosol by 10–25%, in winter. In summer, the variability reduction is in the order of 10%, for backscatter values, it is even increasing by 6%. For the PBL heights, it is the other way round with no variability reduction in winter and 20% reduction in summer.

This result is not surprising, since the individual values in the annual cycle already showed that the aerosol load can change totally from day to day. This is obviously depending on the history of the air mass transported to the measurement site. Therefore, an analysis of the origin of the probed air mass has been made using back trajectories calculated by the German Weather Service (for details on the calculation, see [Kottmeier and Fay, 1998](#)). This analysis has been restricted to aerosol extinction measurements. These values are much more reliable than the backscatter values because no calibration has to be made and the lidar ratio does not have to be guessed. From the back trajectories, only data 36 h before the arrival of the air mass at 13:00 UT on the measurement day has been taken.

Seven classes have been defined, representing the origin of the air mass, namely, northwest (NW), west (W), southwest (SW), southeast (SE), east (E), northeast (NE) and “local.” The class “local” represents very short trajectories with an air parcel staying for a long time close to Hamburg. Each of the seven classes contains only between 7 (SE) and 21 (NW) measurements. Therefore, a further separation into summer and winter (which would certainly be useful) has not been made in order to maintain statistical significance. The result can be seen in [Fig. 13](#). Class “local” has the highest value, which is due to the fact that these measurements were connected with low wind speed and high-pressure situations. These circumstances are favorable for a high aerosol accumulation. Air masses from northerly directions represent lower aerosol extinction (they come over the Atlantic Ocean) than those from southerly directions (they come over the European continent). The variability of the values within one sector is generally reduced compared to the overall value (exception: SE). For the aerosol extinction, the mean standard deviation is reduced by 20%, for the optical depth, by 25%. However, the standard deviations remain high with values between 28% (E) and 81% (SE). For the values of the individual sectors, see [Table 9](#).

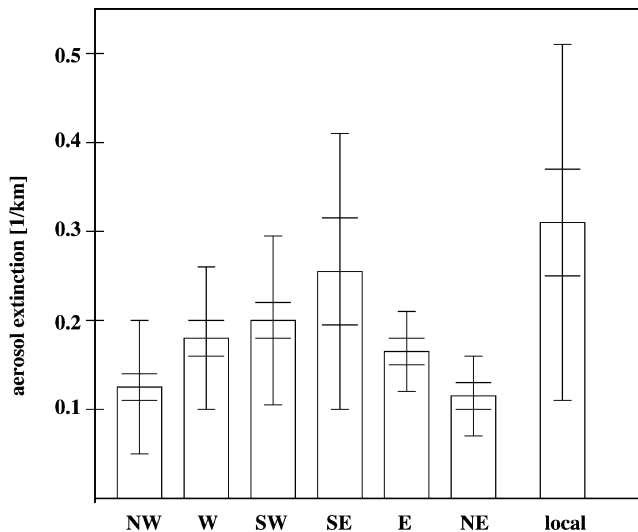


Fig. 13. Mean aerosol extinction depending on the origin of the air mass. Inner error bars represent the standard deviation of the average, outer error bars of individual value.

Table 9

Relative standard deviation of aerosol extinction and optical depth after assignment of the individual values to sectors of air mass origin

Relative standard deviation within sectors								
Category	All	NW	W	SW	SE	E	NE	Local
Aerosol extinction	0.65	0.59	0.46	0.46	0.81	0.28	0.38	0.64
Optical depth	0.82	0.54	0.69	0.67	0.94	0.37	0.51	0.58

Looking for a dependence of the measured lidar ratio on the origin of the air mass, no clear hints as for the aerosol extinction could be found. Measurements belonging to the NW sector showed values ca. 30% lower than the mean, which is not surprising and confirm the model results that show lowest lidar ratios in connection with sea salt aerosols. All easterly sectors belonging to more continental aerosols showed higher values than the mean. NE and SE were ca. 30% higher and E was enhanced by 12%. However, with a standard deviation of 54% for the individual values, this result is only of significance on the average. Almost all classes remain with high variability, on the average, the standard deviation in the classes is with 51% only slightly lower than that of all values (54%). A remarkable reduction of 48% of the standard deviation can be found for the local trajectories. This indicates that those aerosols are well defined and did not underlie a variety of modification processes before they reached the measurement site.

The air mass analysis can, as the separation into seasons, explain part of the variability of the measured aerosol extinction. The next step will be a separate air mass analysis for summer and winter months. This has not been done here because the number of measurements within one class would get too small to remain statistically significant when introducing seven winter and seven summer classes. To explain all variations, more sophisticated models that include aerosol formation, coagulation and sedimentation, hygroscopical growth, aerosol modification by clouds and washout by rain must be used. A more detailed “history” of the aerosols than that given by the trajectories could also be derived by using underlying emission maps.

7. Summary and conclusions

Three years of regular aerosol extinction and backscatter measurements at Hamburg with the MPI Raman lidar at 351 nm have been used for statistical investigations of the aerosol in the boundary layer. The distribution shows most extinction values between 1×10^{-4} and $3 \times 10^{-4} \text{ m}^{-1}$, most backscatter values are between 2×10^{-6} and $6 \times 10^{-6} (\text{m sr})^{-1}$. Higher values occur mainly in summer, lower values in winter. The distributions have positive skewness with high values being more frequent than low ones and can best be represented by lognormal distributions. The planetary boundary layer follows a sinusoidal dependence on season quite good with lowest values of ca. 900 m in December/January and highest values of ca. 2000 m in June/July. Its frequency distribution is Gaussian. The optical depth and the integrated backscatter show higher fluctuations and more pronounced seasonal cycles since they combine aerosol and PBL statistics.

Aerosol extinction and backscatter as well as PBL height have high standard deviations of 40% and more. The values can change quite rapidly with a different air mass advected to the measurement site. Connecting back trajectories with the measured aerosol extinction, a clear dependence of the extinction on the origin of the air mass has been found. Low values are associated with northerly and high values with southerly flows. Highest values are observed under high-pressure conditions connected with very short back trajectories.

Under cloud-free conditions, lidar ratio profiles could be determined, with most values lying between 20 and 90 sr. The values are close to those predicted by Mie calculations for typical aerosols in northern Germany. The measured values give slightly higher mean values, which is especially due to the non-Gaussian distribution with very high values being more frequent than very low ones. The median, which is ca. 10–15% lower than the mean, is more representative for the most probable values.

This lidar ratio statistics is a very valuable tool for the evaluation of pure backscatter measurements, e.g. from aircraft or in future from satellites, to get at least most likely values of the lidar ratio for more precise evaluations of these measurements. The observed high variability of all aerosol parameters will make the reliable evaluation of those measurements a challenging problem.

An aerosol Raman lidar has proven to be a very useful tool for the quantitative determination of the aerosol load from ground at a certain site. Regular measurements over a period of 3 years or more give numbers on the average aerosol distribution that can be used as input for climate models. Additionally, a lidar ratio data base can be built up to obtain some information on probable values. The measurement period will be extended to almost 5 years within the EARLINET project (Bösenberg et al., 2001), including 15 additional stations in the whole Europe.

Acknowledgements

This work was partly funded by the BMBF, project no. 07AF108/7. The intercomparison data from the IfT has been provided by Ulla Wandinger, that from the MIM by Matthias Wiegner. We would like to thank the crew of the Meteorologisches Observatorium Lindenberg of the German Weather Service for the excellent support during LACE'98 and for the star photometer measurements, with special thanks to Ulrich Leiterer. The back trajectories have also been provided by the German Weather Service, thanks to Barbara Fay.

References

- Ackermann, J., 1998. The extinction-to-backscatter ratio of tropospheric aerosols: a numerical study. *J. Atmos. Oceanic Technol.* 15, 1043–1050.
- Althausen, D., Müller, D., Ansmann, A., Wandinger, U., Hube, H., Clauer, E., Zörner, S., 2000. Scanning six-wavelength eleven-channel aerosol lidar. *J. Atmos. Oceanic Technol.* 17, 1469–1482.
- Ansmann, A., 2002. Lindenberg Aerosol Characterization Experiment (LACE'98): overview and main results. *J. Geophys. Res.* 107, in press.

- Ansmann, A., Riebesell, M., Wandinger, U., Weitkamp, C., Voss, E., Lahmann, W., Michaelis, W., 1992a. Combined Raman elastic-backscatter LIDAR for vertical profiling of moisture, aerosol extinction, backscatter, and LIDAR ratio. *Appl. Phys. B* 55, 18–28.
- Ansmann, A., Wandinger, U., Riebesell, M., Weitkamp, C., Michaelis, W., 1992b. Independent measurement of extinction and backscatter profiles in cirrus clouds by using a combined Raman elastic-backscatter lidar. *Appl. Opt.* 31, 7113–7131.
- Bates, T., Huebert, B., Gras, J., Griffiths, F., Durkee, P., 1998. International Global Atmosphere Chemistry (IGAC) Project's First Aerosol Characterization Experiment (ACE 1): overview. *J. Geophys. Res.*, 103.
- Bodhaine, B., Wood, N., Dutton, E., Slusser, J., 1999. On Rayleigh optical depth calculations. *J. Atmos. Oceanic Technol.* 16, 1854–1861.
- Bösenberg, J., Brassington, D., Simon, P. (Eds.), 1997. Instrument Development for Atmospheric Research and Monitoring. Lidar Profiling, DOAS and Tunable Diode Laser Spectroscopy. Transport and Chemical Transformation of Pollutants in the Troposphere, vol. 8. Springer, Berlin.
- Bösenberg, J., Böckmann, C., Eixmann, R., Matthias, V., Mattis, I., Trickl, T., Wiegner, M., 1998. Lidar network to establish an aerosol climatology. 19th International Laser Radar Conference, Annapolis, USA., 23–24.
- Bösenberg, J., Alpers, M., Althausen, D., Ansmann, A., Böckmann, C., Eixmann, R., Franke, A., Freudenthaler, V., Giehl, H., Jäger, H., Kreipl, S., Linné, H., Matthias, V., Mattis, I., Müller, D., Sarközi, J., Schneidenbach, L., Schneider, J., Trickl, T., Vorobieva, E., Wandinger, U., Wiegner, M., 2001. The German Aerosol Lidar Network: Methodology, Data, Analysis, MPI-Report 317. Max-Planck-Institut für Meteorologie, Hamburg.
- Elterman, L., 1968. UV, visible, and IR attenuation for altitudes to 50 km, 1968. *Environmental Research Papers* 285, AFCRL-68-0153, Air Force Cambridge.
- Fernald, F.G., 1984. Analysis of atmospheric lidar observations: some comments. *Appl. Opt.* 23, 652–653.
- Fernald, F.G., Herman, B.M., Reagan, J.A., 1972. Determination of aerosol height distributions by lidar. *J. Appl. Meteorol.* 11, 482–489.
- Grund, C.J., Eloranta, E.W., 1991. University of Wisconsin high spectral resolution lidar. *Opt. Eng.* 30, 6–12.
- Gutkowicz-Krusin, D., 1993. Multiangle lidar performance in the presence of horizontal inhomogeneities in atmospheric extinction and scattering. *Appl. Opt.* 32, 3266–3272.
- Herman, J.R., Barthia, P., Torres, O., Hsu, C., Sefior, C., Celarier, E., 1997. Global distribution of UV-absorbing aerosols from Nimbus 7/TOMS data. *J. Geophys. Res.* 102 (D14), 16911–16922.
- Holben, B.N., Eck, T.F., Slutsker, I., Tanré, D., Buis, J.P., Setzer, A., Vermote, E., Reagan, J.A., Kaufman, Y.J., Nakajima, T., Lavenü, F., Jankowiak, I., Smirniiov, A., 1998. AERONET—a federated instrument network and data archive for aerosol characterization. *Remote Sens. Environ.* 66, 1–16.
- IPCC, 2001. *Climate change 2001: the science of climate change. Technical Summary of the Working Group I Report*, World Meteorological Organization, Genf.
- Johnson, N., Leone, F.C., 1964. *Statistics and Experimental Design in Engineering and the Physical Sciences*, vol. 1. Wiley, New York.
- Kaufman, Y.J., Tanré, D., Gordon, H., Nakajima, T., Lenoble, J., Frouin, R., Graßl, H., Herman, B., King, M., Teillet, P.M., 1997. Passive remote sensing of tropospheric aerosol and atmospheric correction for the aerosol effect. *J. Geophys. Res.* 102 (D14), 16815–16830.
- Klett, J.D., 1981. Stable analytical inversion solution for processing lidar returns. *Appl. Opt.* 20, 211–220.
- Kottmeier, C., Fay, B., 1998. Trajectories in the Antarctic lower troposphere. *J. Geophys. Res.* 103 (D9), 10947–10959.
- Kovalev, V.A., Moosmüller, H., 1994. Distortion of particulate extinction profiles measured with lidar in a two-component atmosphere. *Appl. Opt.* 33, 6499–6507.
- Matsumoto, M., Takeuchi, N., 1994. Effects of misestimated far-end boundary values on two common lidar inversion solutions. *Appl. Opt.* 33, 6451–6456.
- Russell, P.B., Hobbs, P.V., Stowe, L., 1999. Aerosol properties and radiative effects in the United States East Coast haze plume: an overview of the Tropospheric Aerosol Radiative Forcing Observational Experiment (TARFOX). *J. Geophys. Res.* 104 (D2), 2213–2222.
- Sasano, Y., Browell, E.V., Ismail, S., 1985. Error caused by using a constant extinction/backscattering ratio in the lidar solution. *Appl. Opt.* 24, 3929–3932.
- Shipley, S.T., Tracy, D.H., Eloranta, E.W., Trauger, J.T., Sroga, J.T., Roesler, F.L., Weinman, J.A., 1983. High

spectral resolution lidar to measure optical scattering properties of atmospheric aerosols: 1. Theory and instrumentation. *Appl. Opt.* 22, 3716–3732.

- Wandinger, U., Müller, D., Böckmann, C., Althausen, D., Matthias, V., Bösenberg, J., Weiß, V., Fiebig, M., Wendisch, M., Stohl, A., Ansmann, A., 2002. Optical and microphysical characterization of biomass-burning and industrial-pollution aerosols from multiwavelength lidar and aircraft measurements. *J. Geophys. Res.*, 107, in press.
- Whiteman, D., 1999. Application of statistical methods to the determination of slope in lidar data. *Appl. Opt.* 38 (15), 3360–3369.
- Wiegner, M., Quenzel, H., Rabus, D., Völker, W., Völger, P., Ackermann, J., Köhler, C., Fergg, F., Wildgruber, G., 1995. The mobile three-wavelength backscatter lidar of the Meteorological Institute of the University of Munich. *Lidar Atmos. Sens.*, vol. 2505. SPIE, Bellingham, WA, pp. 2–10.